SNAP-tag-enabled super-resolution imaging reveals constitutive and agonist-dependent trafficking of GPR56 in pancreatic β-cells

Olaniru, Oladapo; Cheng, Jordan; Ast, Julia; Arvaniti, Anastasia; Atanes, Patricio; Huang, GC; King, Aileen; Jones, Peter; Broichhagen, Johannes; Hodson, David; Persaud, Shanta J

[Link to publication on Research at Birmingham portal](#)

SNAP-tag-enabled super-resolution imaging reveals constitutive and agonist-dependent trafficking of GPR56 in pancreatic β-cells

Oladapo E. Olaniru [1,*], Jordan Cheng [2], Julia Ast [3,4], Anastasia Arvaniti [3,4], Patricio Atanes [1], Guo C. Huang [1], Aileen J.F. King [1], Peter M. Jones [1], Johannes Broichhagen [5], David J. Hodson [3,4], Shanta J. Persaud [1,**]

ABSTRACT

Objective: Members of the adhesion G protein-coupled receptor (aGPCR) subfamily are important actors in metabolic processes, with GPR56 (ADGRG1) emerging as a possible target for type 2 diabetes therapy. GPR56 can be activated by collagen III, its endogenous ligand, and by a synthetic seven amino-acid peptide (TYFAVLM; P7) contained within the GPR56 Stachel sequence. However, the mechanisms regulating GPR56 trafficking dynamics and agonist activities are not yet clear.

Methods: Here, we introduced SNAPf-tag into the N-terminal segment of GPR56 to monitor GPR56 cellular activity *in situ*. Confocal and super-resolution microscopy were used to investigate the trafficking pattern of GPR56 in native MIN6 β-cells and in MIN6 β-cells where GPR56 had been deleted by CRISPR-Cas9 gene editing. Insulin secretion, changes in intracellular calcium, and β-cell apoptosis were determined by radioimmunoassay, single-cell calcium microfluorimetry, and measuring caspase 3/7 activities, respectively, in MIN6 β-cells and human islets.

Results: SNAP-tag labelling indicated that GPR56 predominantly underwent constitutive internalisation in the absence of an exogenous agonist, unlike GLP-1R. Collagen III further stimulated GPR56 internalisation, whereas P7 was without significant effect. The overexpression of GPR56 in MIN6 β-cells did not affect insulin secretion. However, it was associated with reduced β-cell apoptosis, while the deletion of GPR56 made MIN6 β-cells more susceptible to cytokine-induced apoptosis. P7 induced a rapid increase in the intracellular calcium in MIN6 β-cells (in a GPR56-dependent manner) and human islets, and it also caused a sustained and reversible increase in insulin secretion from human islets. Collagen III protected human islets from cytokine-induced apoptosis, while P7 was without significant effect.

Conclusions: These data indicate that GPR56 exhibits both agonist-dependent and -independent trafficking in β-cells and suggest that while GPR56 undergoes constitutive signalling, it can also respond to its ligands when required. We have also identified that constitutive and agonist-dependent GPR56 activation is coupled to protect β-cells against apoptosis, offering a potential therapeutic target to maintain β-cell mass in type 2 diabetes.

1. INTRODUCTION

Adhesion G-protein coupled receptors (aGPCRs) are atypical GPCRs with an unusually large extracellular domain, containing motifs that enable them to participate in cell—cell adhesion. A unique feature of aGPCRs is the presence of a 'GPCR Autoproteolysis INducing' (GAIN) domain, in which, in most cases, an N-terminal fragment is autocatalytically cleaved from the receptor [1]. The N-terminal fragment remains joined non-covalently to the seven-transmembrane portion of the receptor at the GPCR proteolytic site within the GAIN domain [2]. Though aGPCRs are the second largest class of GPCRs, they remain one of the least studied despite their involvement in many physiological

processes, as the majority are orphans, for which endogenous ligands have not yet been identified.

It has been established that the unique structural features of aGPCRs enable them to exhibit complex signalling properties, and three distinct signalling mechanisms have been described thus far. First, downstream signalling of aGPCRs can occur when the N-terminal fragment dissociates by either agonist binding or mechanical detachment [3,4]. Second, removing the N-terminal fragment exposes a built-in tethered agonist called 'Stachel', located at the uppermost part of the first transmembrane domain [5]. The exposure of the Stachel sequence, or the addition of a synthetic peptide representing the native Stachel sequences, activates aGPCRs *in vitro* [6—10]. Third, there have been

[1]Department of Diabetes, School of Life Course Sciences, King's College London, Guy's Campus, London SE1 1UL, UK [2]Department of Imaging Chemistry and Biology, School of Biomedical Engineering & Imaging Sciences, 4th floor Lambeth Wing, St Thomas' Hospital, London, SE1 7EH, UK [3]Institute of Metabolism and Systems Research (IMSR), Centre of Membrane Proteins and Receptors (COMPARE), University of Birmingham, Birmingham, UK [4]Centre for Endocrinology, Diabetes and Metabolism, Birmingham Health Partners, Birmingham, UK [5]Leibniz-Forschungsinstitut für Molekulare Pharmakologie (FMP), Robert-Rössle-Str. 10, 13125, Berlin, Germany

*Corresponding author. E-mail: oladapo.e.olaniru@kcl.ac.uk (O.E. Olaniru).

**Corresponding author. E-mail: shanta.persaud@kcl.ac.uk (S.J. Persaud).

Original Article

demonstrations of Stachel-independent agonism and instances of Stachel-induced signalling occurring from conformational changes following agonist binding rather than by removing the N-terminal segment [11,12]. However, despite a general understanding of aGPCR activation mechanisms, it is unclear how aGPCRs are trafficked from the plasma membrane after activation.

GPCR trafficking, a mechanism that determines the number of receptors available at the cell membrane for agonist binding, is well documented for the typical rhodopsin-like and class B GPCRs. Thus, receptor internalisation occurs upon ligand binding, resulting in receptor-specific desensitisation. Once internalised, receptors are transported to the endosomes, in which they continue to signal [13], undergo degradation, or are recycled back to the plasma membrane for further rounds of receptor signalling. More recently, GPCR trafficking has been investigated using SNAP-tag technology, in which a modified DNA repair enzyme, human O^6-alkylguanine-DNA-alkyltransferase, is fused to the N-terminal segment of a GPCR and reacts with O^6-benzylguanine-conjugated fluorophores, permitting the visualisation of the GPCR. This approach has been used to identify the activation and internalisation of class A and B GPCRs involved in metabolism, including the growth hormone secretagogue-receptor 1a (GHS-R1a) [14] and glucagon-like peptide-1 (GLP-1) receptor, respectively [15—17]. Studies reporting the ligand-induced down-regulation of GPR56 and CD97, another aGPCR, indicate that aGPCRs might follow similar patterns of signal inactivation [18—20], but there is no information on the trafficking of any aGPCRs to the best of our knowledge.

GPR56, a member of the aGPCR family, is broadly expressed in tissues, and we have identified that it is the most abundant islet-expressed GPCR [21,22]. GPR56 is activated by collagen III, its endogenous ligand [23], and a synthetic peptide, TYFAVLM (P7), which is present in the N-terminal Stachel sequence of GPR56 [10]. We and others have shown that the exposure of islets to collagen III led to increased insulin secretion and protection against apoptosis in a GPR56-dependent manner [24,25]. We have now used SNAP-tag technology combined with advanced imaging and novel SNAP labels to investigate the activation and internalisation of GPR56 in MIN6 β-cells and identify the trafficking patterns elicited by collagen III and P7. We have compared GPR56 trafficking in β-cells to the prototypical class B GPCR, GLP-1R. We have also determined the functional effects of the P7 activation of GPR56 on calcium mobilisation, insulin secretion, and apoptosis using isolated human islets.

2. MATERIALS AND METHODS

2.1. Materials

The following consumables were used: a jetPRIME® transfection reagent from PolyPlus Transfection (Illkirch, France) and Lipofectamine® 2000 Transfection Reagent from Thermo Fisher Scientific (Loughborough, UK). TYFAVLM (P7) was synthesised by Pepceuticals (Enderby, UK) and purchased (catalogue number SML1773) from Sigma (Dorset, UK). Caspase-Glo 3/7 assay kits, anti-mouse IgG (H+L) HRP-conjugated secondary antibody, and ECL western blotting reagent were purchased from Promega (Southampton, UK), μ-Slide 8-well from Ibidi (Grafelfing, Germany), TNF-α, IL-1β, and IFN-γ from PeproTech (London, UK), mouse monoclonal anti-GPR56 antibody (MABN310) from Millipore (Gillingham, UK), Gpr56 double nickase plasmid (sc-420657-NIC) and mouse anti-β-actin (C4) antibody from Santa Cruz Biotechnology (Heidelberg, Germany), transferrin receptor antibody conjugated with Alexa fluor® 488 (BS-0988R-A488) from Stratech (Cambridge, UK), CellLight® Early Endosomes Rab5-GFP,

BacMam 2.0 from Thermo Fisher Scientific (Loughborough, UK), GPR56 and GAPDH QuantiTech qPCR primers from Qiagen (Manchester, UK), MemBrite™ Fix 640/660 Cell Surface Staining Kit from Biotium (Fremont, USA), soluble recombinant collagen III from Abcam (Cambridge, UK), SNAP-Surface® 549 from NEB (Hitchin, UK), and SNAP_GLP1R plasmid from Cisbio (Codolet, France). BG-TMR and SBG-SiR [17] were provided by Professor David Hodson (University of Birmingham) and Dr. Johannes Broichhagen (Leibniz FMP, Berlin). Mouse Gpr56 plasmid was provided by Professor Xianhua Piao (University of California). All other reagents, including cell culture media, were purchased from Sigma—Aldrich (Dorset, UK).

2.2. Cell lines and human islets

HEK293 cells with improved adhesion properties (AD293 cells) and MIN6 β-cells (Mycoplasma free; obtained from Agilent and J.I. Miyasaki, Osaka University Japan, respectively) were maintained in a culture in Dulbecco's Modified Eagle's Medium (DMEM) and supplemented with 10% FBS, 1% L-glutamine, and 100 U/ml penicillin/0.1 mg/ml streptomycin at 37 °C in a humidified chamber. Gpr56KO-MIN6 β-cells were maintained in the same medium, supplemented with 1.5 μg/ml puromycin. Human islets for functional studies were isolated at King's College Hospital, London, from 5 non-diabetic donors (Suppl. Table 1), with appropriate ethical approval.

2.3. SNAP-tag plasmid construction

SNAPf-tag [26] was cloned into the N-terminal segment of full-length untagged mouse Gpr56 plasmid immediately downstream from the signal peptide to form the SNAP_Gpr56 plasmid. Briefly, mouse Gpr56 was amplified with 5′-AGCCCCCGAGAAGACTTC-3′ and 5′-GCCACTGTGTGCACCTTG-3′ primers, whereas SNAPf was amplified with 5′-TGCAAGGTGCACACAGTGGCGCCGGCATCGATGCCATC-3′ and 5′-CGGAAGTCTTCTCGGGGGGCTGATATCGCCCAGGCCTGG-3′ primers. PCR products were checked for size on agarose gel, and the DNA fragments were combined via Gibson Assembly cloning [27]. The success of the cloning was confirmed by Sanger sequencing (Suppl. Fig. 1a & 1b).

2.4. CRISPR-Cas9 deletion of Gpr56 in MIN6 β-cells

MIN6 β-cells were transfected with 1 μg Gpr56 double nickase plasmids containing a mutated Cas9 nuclease and a target-specific 20 nt gRNA using jetPRIME®. The region of the Gpr56 gene targeted by the gRNA was TAGAGGGCTCTATCAC. Cells were maintained in culture in DMEM containing 1.5 μg/ml puromycin to allow for the selection of transformed cells. Single colonies were selected using the cell dilution method [28] and expanded in 96-well plates. DNA was extracted from each clone, and the region flanking the deleted segment was amplified by PCR using the forward primer AGCG-GAACCAGACCCAACA and reverse primer GGGCTTTCCATGTCTTCCGT. The gRNA-induced double-strand breaks with a deletion of 16 bp at exon 3 of Gpr56 in MIN6 β-cells, confirmed by Sanger sequencing. The deletion of GPR56 in Gpr56KO-MIN6 β-cells was confirmed by western blotting.

2.5. Western blotting

Groups of 7×10^5 Gpr56KO-MIN6 β-cells, native MIN6 β-cells or MIN6 β-cells with or without GPR56 overexpression were lysed in a radioimmunoprecipitation assay (RIPA) buffer at 4 °C for 30 min in the presence of phosphatase and protease inhibitors, and protein contents were determined by BCA assay [29]. For this purpose, 50 μg of protein lysates was boiled in Laemmli sample buffer and fractionated on 4—12% polyacrylamide gels before being electrotransferred to PVDF

membranes at 30 V overnight at 4 °C. PVDF membranes were blocked with 5% BSA in Tris-buffered saline, 0.1% Tween-20, pH 7.6 (TBST) for 1 h and probed overnight with a mouse monoclonal anti-GPR56 antibody (1:500) and a mouse monoclonal anti-β-actin antibody (1:1000), before being incubated with an anti-mouse HRP-conjugated secondary antibody (1:2500). Protein bands were revealed with an X-ray film exposure after the addition of the ECL substrate, and protein densities were quantified by ImageJ.

2.6. Identification of GPCR localisation in transiently transfected fixed cells by SNAP-tag labelling

AD293 and MIN6 β-cells or *Gpr56*KO-MIN6 β-cells, seeded at a density of 8×10^4 cells/well of an 8-well μ-slide, were transfected with SNAP_*Gpr56* or SNAP_*Glp1r* plasmids using a jetPRIME® reagent. Briefly, a transfection mix of 100 ng DNA plasmid and jet-PRIME® reagent at a ratio of 3:1 was allowed to stand for 15 min at room temperature before it was added to the cells in drops. Trans-fected cells were maintained in the culture for 24−48 h. Cells transiently transfected with untagged full-length mouse *Gpr56* plasmid were used as negative controls. Receptor localisation was identified by exposing transfected cells to SNAP-tag substrates (0.5 μmol/l BG-TMR, SNAP-Surface® 549, or SBG-SiR) for 30 min at 37 °C. Cells were fixed for 10 min in 4% paraformaldehyde at 4 °C. Nuclei were identified with DAPI staining, and plasma membranes were identified by staining with MemBrite™ Fix, according to the manufacturer's protocol. Images were acquired using an A1 inverted confocal microscope with a 60x/1.4 NA oil objective with excitation at 561 nm for BG-TMR/SNAP-Surface® 549 and 640 nm for SBG-SiR/MemBrite™ Fix, whereas emitted signals were collected at 570−614 nm and 670−715 nm, respectively. All directly compared images were acquired under the same conditions, and they were analysed by ImageJ software. Percentage internalisation was determined by expressing the corrected fluorescence of the internalised GPCRs as a fraction of the corrected total cellular fluorescence [30]. Briefly, an outline was drawn around each cell and their cytoplasm, and the area, mean fluorescence, and integrated densities of the entire cell and cytoplasm were measured. Multiple background fluorescence readings were also taken. The total cell fluorescence was obtained by the following equation : corrected total cell fluorescence = integrated density — (area of selected cell x mean fluorescence of background readings). The corrected fluorescence of the internalised receptors was obtained in the same way, instead of using the mean fluorescence from the cytoplasm.

2.7. Immunofluorescence endosomal staining

SNAP_*Gpr56*-MIN6 β-cells were incubated overnight at 37 °C with a BacMam 2.0 virus containing a fusion construct of the early endosomal marker Rab5a with emerald GFP. Then, the cells were labelled with 0.5 μmol/l SNAP-Surface® 549 substrate for 30 min. Cells were fixed in 4% paraformaldehyde for 10 min at 4 °C and washed in PBS. The nuclei were stained with DAPI. In parallel experiments, fixed SNAP_*Gpr56*-MIN6 β-cells were incubated at 4 °C overnight with a transferrin receptor antibody (1:50) to track endocytosis and recycling, then washed in PBS. Imaging was carried out with a 60x/1.4 NA oil objective using an A1 inverted confocal microscope with excitation at 488 nm for Rab5-GFP and transferrin receptor and 561 nm for SNAP-Surface® 549. The emitted fluorescence was detected at 515−545 nm and 570−614 nm, respectively. Colocalisation of internalised SNAP_GPR56 with Rab5a-GFP or transferrin receptors was determined using the EzColocalisation plugin in ImageJ [31], and Mander's correlation coefficient (MCC) was quantified [32] to determine the fraction of SNAP_GPR56 in the cytoplasm that colocalised with Rab5a or transferrin receptors.

2.8. Super-resolution live cell imaging of constitutive GPR56 trafficking

Transfected MIN6 β-cells or *Gpr56*KO-MIN6 β-cells were labelled with 0.5 μmol/l SNAP-Surface® 549 substrate for 30 min at 37 °C in FBS-free DMEM. After two washes in PBS, images were taken on a Nikon Eclipse Ti-2 instant structured illumination microscope (iSIM). Excitation was delivered at 561 nm through a 100x/1.49 NA oil objective, and emitted signals were collected at 570−614 nm using a Hamamatsu Flash4.0 sCMOS camera. Deconvolution was carried out using a 2D Richardson-Lucy algorithm on NIS-element AR software. Particles were tracked by the TrackMate plugin in ImageJ [33], which applies Laplacian of Gaussian filtering before detecting local maxima for the spot signal. We excluded spots with a low-quality signal by setting the particle diameter to 0.5 μm and a threshold of 5.

2.9. Agonist-induced GPR56 and GLP1R internalisation

MIN6 β-cells or *Gpr56*KO-MIN6 β-cells were transiently transfected with SNAP_*Glp1r* or SNAP_*Gpr56*, respectively, and maintained in DMEM supplemented with 10% FBS, 1% L-glutamine and 100U/ml penicillin/0.1 mg/ml streptomycin. The cells were labelled with 0.5 μmol/l SNAP-Surface® 549 substrate for 30 min at 37 °C before being stimulated with GPR56 agonists (100 nmol/l collagen III or 1 mmol/l P7), a GLP1R agonist (100 nmol/l exendin-4), or a vehicle control for a further 30 min. Cells were fixed in 4% paraformaldehyde at 4 °C, and nuclei were stained with DAPI. Images were captured using an A1 inverted confocal microscope using a 60x/1.4 NA oil objective with excitation delivered at 561 nm and emission at 570−614 nm for SNAP-Surface® 549 and 355 nm for DAPI with emission at 420−480 nm. Images were analysed by ImageJ, and the percentage internalisation was determined by expressing the corrected fluorescence of internalised GPCRs as a fraction of corrected total cellular fluorescence, as previously described [30].

2.10. Functional effects of GPR56 overexpression in MIN6 β-cells

2.10.1. Transient overexpression of Gpr56

Groups of 3×10^5 MIN6 β-cells were seeded into 6-well plates and incubated overnight at 37 °C in DMEM supplemented with 10% FBS, 1% L-glutamine, and 100 U/ml penicillin/0.1 mg/ml streptomycin. Cells were transiently transfected with 0.12 μg and 1.2 μg of full-length *Gpr56* plasmid for 24 and 48 h using Lipofectamine® 2000 (1:15), and the degree of *Gpr56* overexpression was determined by qPCR relative to *Gapdh* mRNA levels in the same samples. MIN6 β-cells transiently transfected with 1200 ng of an empty pcDNA3 vector were used as controls. Briefly, RNAs were extracted from MIN6 β-cells with on-column DNAse digestion, and they were reversed transcribed to cDNAs. Quantitative PCR was carried out using SYBR green and Qiagen QuantiTect primers to determine the expression of *Gpr56* and *Gapdh*, as described [21,22]. The dilution factor required to generate a *Gapdh* cycle threshold value of 18 for each cDNA was calculated, and the expression of target gene transcripts was normalised against the reference gene *Gapdh* in the same samples [34]. GPR56 over-expression was also determined by western blotting, as described earlier.

2.10.2. Insulin secretion

Insulin secretion following *Gpr56* overexpression was determined by incubating 30,000 MIN6 β-cells for 48 h after transfection with an empty pcDNA3 vector or *Gpr56* plasmid in 96-well plates in a medium supplemented with 2 mmol/l glucose for 1 h at 37 °C. Insulin secretion was determined by radioimmunoassay [35].

2.10.3. MIN6 β-cell apoptosis

MIN6 β-cells transiently transfected with an empty pcDNA3 vector or MIN6 β-cells that were transfected with *Gpr56* plasmids were cultured in a complete medium for 24 h before being exposed to DMEM containing 2% fetal bovine serum with or without a cytokine cocktail (5 U/μL TNFα, 0.5 U/μL IL-1β, 5 U/μL IFNγ) for another 20 h. In parallel, groups of five human islets were maintained in RPMI supplemented with 10% FBS for 24 h in the presence or absence of P7 or collagen III before being exposed to RPMI containing 2% FBS with or without a cytokine cocktail (5 U/μL TNFα, 0.5 U/μL IL-1β, 5 U/μL IFNγ) in the continued presence of P7 or collagen III for another 20 h. Cells and islets were incubated with a Caspase 3/7 Glo working solution, and caspase 3/7 activities were measured using a Veritas luminometer [36].

2.11. Calcium imaging

Groups of 1×10^6 native β-cells, SNAP_*Gpr56*-MIN6 β-cells, or 300 human islets partially dissociated in Accutase® (400—600units/ml), were seeded onto acid-ethanol-washed coverslips and allowed to adhere overnight at 37 °C in DMEM or RPMI containing 10% FBS, respectively. The cells were incubated with 5 μmol/l of the calcium dye Fura-2AM for 30 min before being perifused with a physiological buffer supplemented with 2 mmol/l glucose, 20 mmol/l glucose, 100 μmol/l P7, 50 μmol/l ATP or 500 μmol/l tolbutamide. Imaging was performed using a Zeiss Axiovert 135 and 20x/0.5NA objective. Excitation was performed alternately at 340 nm and 380 nm, and emitted fluorescence was detected at 500—525 nm. Real-time changes in intracellular calcium were determined as 340/380 nm ratiometric data.

2.12. Dynamic insulin secretion

Groups of 60 human islets were perifused with a physiological salt solution [37] supplemented with 2 mmol/l or 2 0 mmol/l glucose in the absence or presence of 100 μmol/l P7 in a perifusion system maintained at 37 °C. Perifusates were collected every 2 min, and insulin secretion was quantified by radioimmunoassay [35].

2.13. Statistical analyses

Numerical data are expressed as mean ± SEM. All statistical analyses were conducted using GraphPad Prism 8 software. Significance between the two groups was tested using an unpaired Student's t-test, and multiple interactions were determined by a two-way ANOVA with an appropriate posthoc test. Differences between groups were considered statistically significant when p values were <0.05.

3. RESULTS

3.1. GPR56 shows constitutive trafficking

The fluorogenic probe SNAPf [26] was fused into the N-terminal segment of *Gpr56* after the signal peptide to precisely visualise and monitor cellular GPR56 expression (Figure 1A, Suppl. Fig. 1a, and Suppl. Fig. 1b). The SNAP_GPR56 expression at the plasma membrane of MIN6 β-cells labelled with SNAP-Surface® 549 was confirmed using confocal microscopy and a MemBrite™ Fix, a commercially available cell surface staining kit that reacts irreversibly with membrane proteins. Thus, Figure 1B demonstrates that cells transiently transfected with the SNAP_*Gpr56* plasmid showed cell surface staining, consistent with the pattern observed with the addition of the MemBrite™ Fix to the cells. This effect was not due to non-specific staining, as cells transfected with *Gpr56* plasmid and lacking the SNAPf-tag did not show any fluorescent signal (Suppl. Fig. 1c and Suppl. Fig. 1d). However, cytoplasmic staining was also evident in MIN6 β-cells expressing SNAP_*Gpr56* (Figure 1B) and was examined further by the transfection of AD293 cells with SNAP_*Gpr56* and SNAP_*Glp1r* to identify their intracellular localisations. Figure 2A and B indicate that the labelling of AD293 cells transfected with SNAP_*Gpr56* or SNAP_*Glp1r* with a cell-permeable fluorescent label (i.e., BG-TMR) was associated with intense plasma membrane staining, as expected of surface GPCRs. However, AD293 cells expressing SNAP_GPR56 also showed intense intracellular fluorescence, with 46.0 ± 4.6% of labelled receptors in the intracellular compartment in the absence of an agonist (Figure 2A and E). In contrast, GLP1R, a well characterised GPCR reported to have very limited constitutive internalisation [38], showed only minor cytoplasmic staining when SNAP_GLP1R-AD293 cells were labelled with BG-TMR (Figure 2B). These observations suggest constitutive GPR56 internalisation. However, as BG-TMR is cell-permeant, it is possible that the intracellular fluorescence could reflect the labelling of newly synthesised receptors in the cytoplasm. SNAP-Surface® 549, a labelling substrate
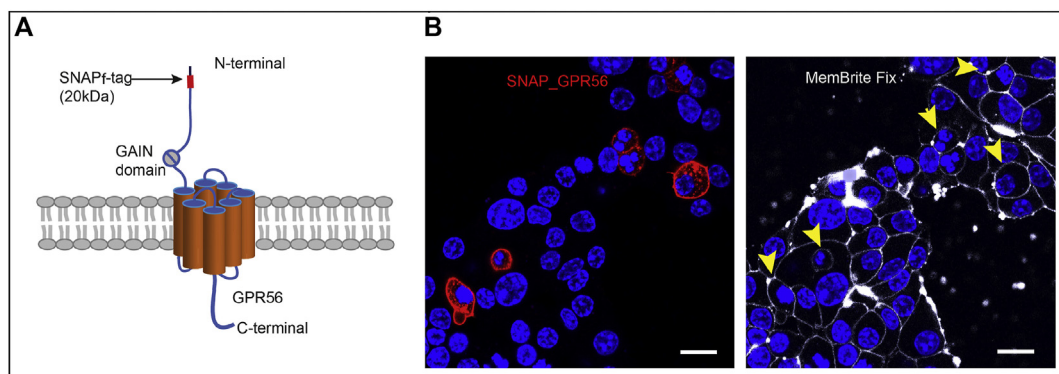
Figure 1: Expression of SNAP_GPR56 at the cell surface. A. Schematic showing the position of the SNAPf tag, just below the GPR56 signal peptide. The image is not drawn to scale. **B**. A representative confocal microscopy image (left) showing localisation of SNAP_GPR56 (red) at the plasma membrane of MIN6 β-cells after labelling with the cell impermeant substrate SNAP-Surface® 549. The image on the right side shows colocalisation of SNAP_GPR56 with the plasma membrane, as revealed by a surface membrane protein dye, Membright™ Fix. Scale bar = 10 μm. Yellow arrowheads show cells expressing SNAP-GPR56 and colocalisation with Membright™ at the plasma membrane.
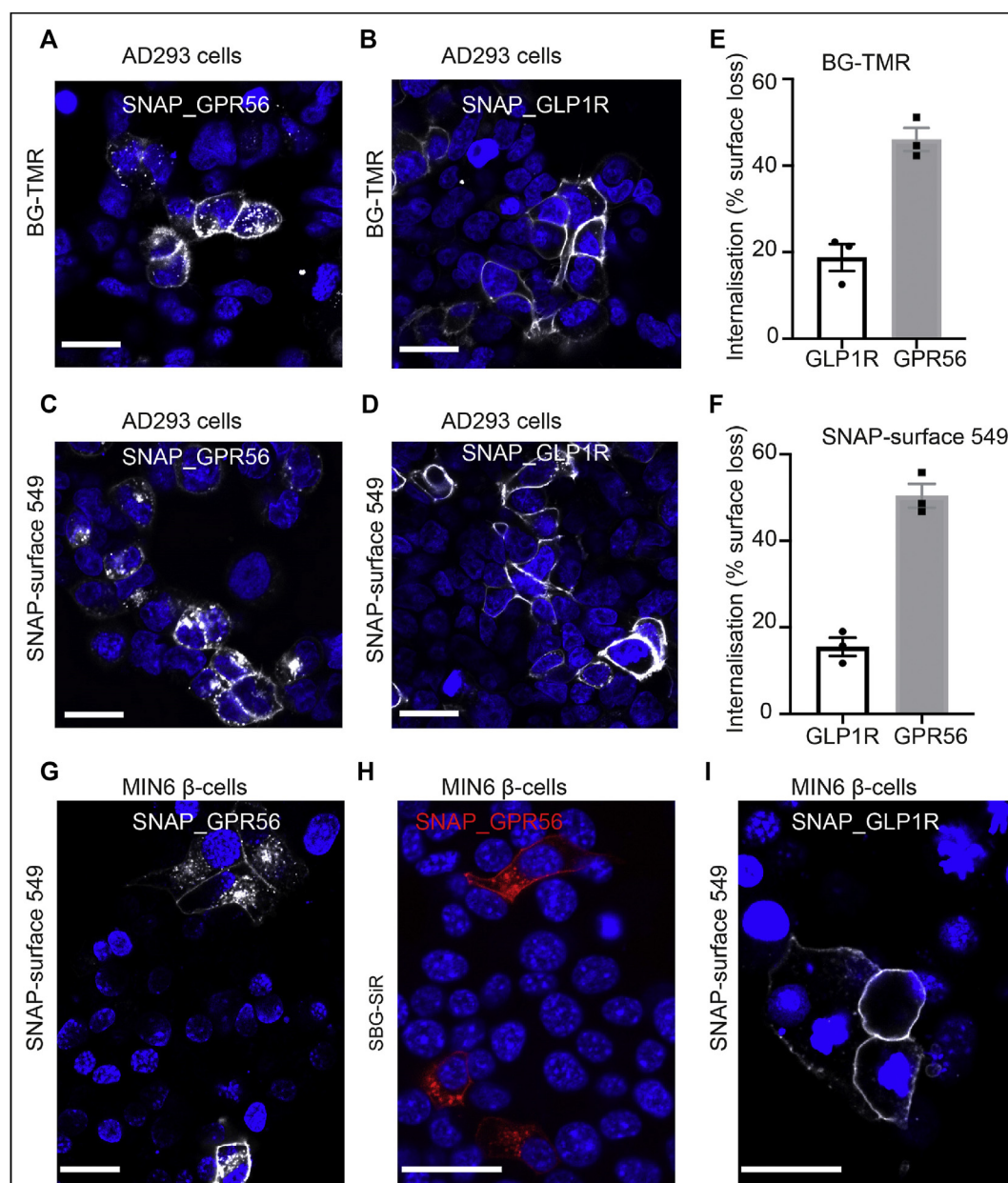
Figure 2: GPR56 displays constitutive trafficking in fixed AD293 and MIN6 β-cells. Fluorescent images showing surface-expressed: **A**. SNAP_GPR56 in AD293 cells following labelling with BG-TMR. **B**. SNAP_GLP1R in AD293 cells following labelling with BG-TMR. **C**. SNAP_GPR56 in AD293 cells following labelling with SNAP-Surface® 549. **D**. SNAP_GLP1R in AD293 cells following labelling with SNAP-Surface® 549. Scale bar a-d = 20 μm **E**. Percentage internalisation of surface GLP1R and GPR56 following labelling with the cell-permeant substrate BG-TMR, mean ± SEM, n = 3 separate experiments. **F**. Percentage internalisation of surface GLP1R and GPR56 following labelling with the cell impermeant substrate SNAP-Surface® 549, mean ± SEM, n = 3 separate experiments. **G**. Confocal image of MIN6 β-cells transfected with SNAP_*Gpr56* and labelled with SNAP-Surface® 549. **H**. Confocal image of MIN6 β-cells transfected with SNAP_*Gpr56* and labelled with SBG-SiR. Scale bar g-h = 20 μm **I** Confocal image of MIN6 β-cells transfected with SNAP_Glp1r and labelled with SNAP-Surface® 549. Scale bar = 20 μm.

used for extracellular staining, was used to identify GPR56 and GLP1R cellular localisation in the absence of agonists to rule out this possibility. Labelling with SNAP-Surface® 549 showed similar results to those obtained with BG-TMR, with GPR56 being expressed both at the plasma membrane and within the cytoplasm, whereas the majority of GLP1R was confined to the plasma membrane in the absence of an agonist (Figure 2C and D). An analysis of multiple transfected AD293 cells revealed that approximately 50% of SNAP_GPR56 was internalised in its unstimulated state, whereas less than 20% of SNAP_GLP1R was

identified within cells under the same conditions (Figure 2E and F). These data suggest that GPR56 possesses high levels of constitutive internalisation.

Having established the SNAP_GPR56 localisation pattern in AD293 cells, we built on our earlier work on *Gpr56* expression and function in islets [21,22,24] to investigate GPR56 trafficking in β-cells. Similar to AD293 cells, the transfection of MIN6 β-cells with SNAP_*Gpr56* and subsequent labelling with SNAP-Surface® 549, or the more recently described completely cell-impermeant and far-red SBG-SiR [17],

showed that GPR56 is localised within the cytoplasm and at the plasma membrane, indicating that the constitutive trafficking of GPR56 occurs irrespective of the cell type (Figure 2G and H). In contrast, the labelling of SNAP_GLP1R expressing MIN6 β-cells with SNAP-Surface® 549 demonstrated that GLP1R showed more limited constitutive trafficking, as expected (Figure 2I).

3.2. Super-resolution live cell imaging confirms GPR56 constitutive trafficking in MIN6 β-cells

We investigated whether the constitutive trafficking of GPR56 seen in fixed AD293 and MIN6 β-cells is a dynamic process by conducting fast

imaging of SNAP_GPR56 in MIN6 β-cells using super-resolution iSIM microscopy (~130 nm lateral resolution). As expected, we observed the dynamic trafficking of SNAP_GPR56 receptors in transfected native MIN6 β-cells, with both membrane and intracellular receptor localisation (Figure 3A). *Gpr56* is expressed endogenously by native MIN6 β-cells [24,25]. Thus, it is possible that the observed constitutive trafficking was due to the increase in the amount of the already high number of GPR56 receptors. Therefore, we generated *Gpr56*KO-MIN6 β-cells, in which *Gpr56* was deleted by CRISPR-Cas9 technology (Suppl. Fig. 2a), and confirmed the absence of GPR56 in our stable cell line by western blotting (Suppl. Fig. 2b and 2c). Native and *Gpr56*KO-
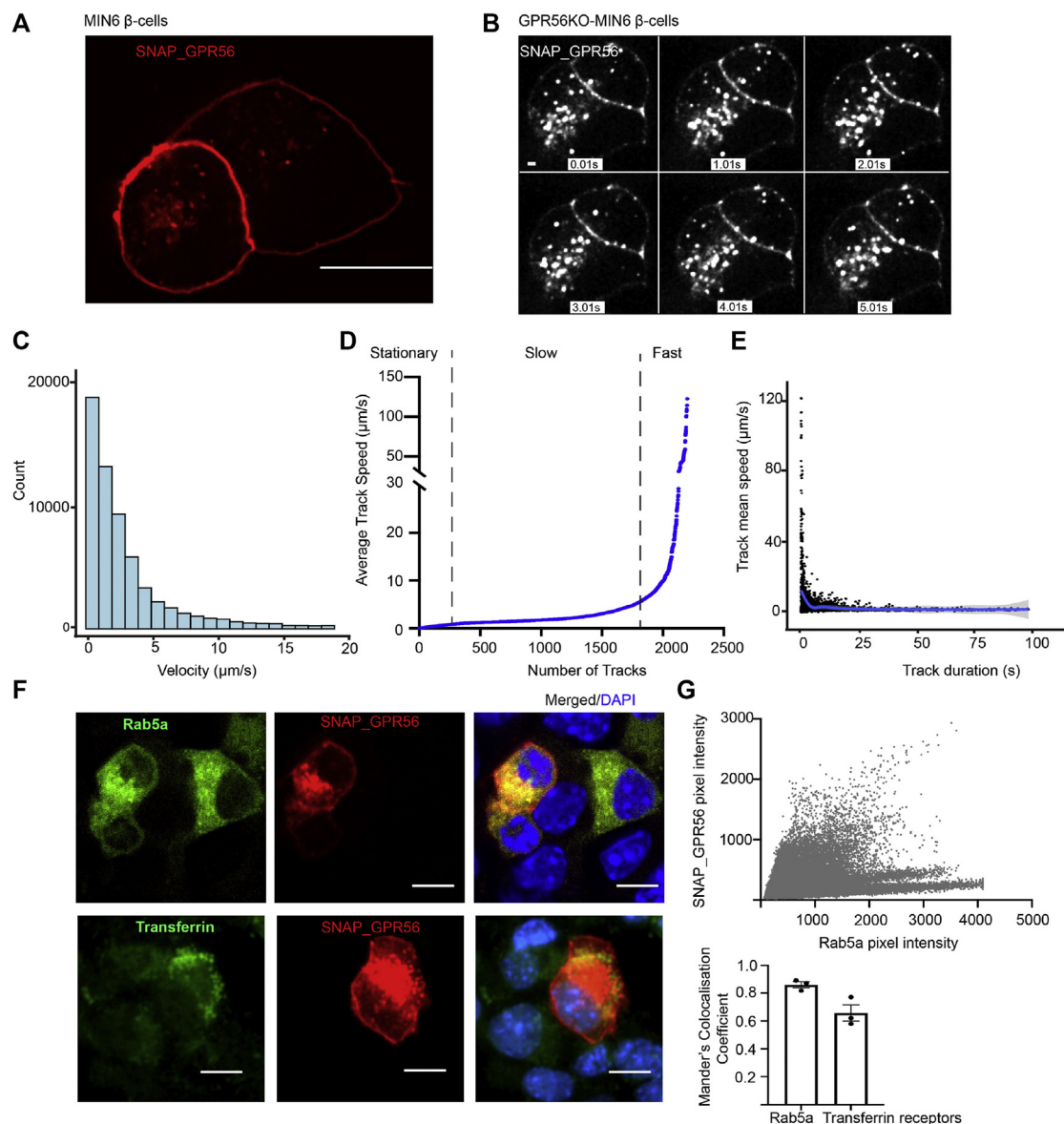
Figure 3: Super-resolution imaging of GPR56 constitutive trafficking in live MIN6 β-cells. A. A single frame from live imaging of native MIN6 β-cells transfected with SNAP_*Gpr56* and labelled with SNAP-Surface® 549. Scale bar = 10 μm **B**. Representative live imaging of SNAP_GPR56 trafficking in *Gpr56*KO-MIN6 β-cells. The first 5 s are shown. Scale bar = 1 μm **C**. Velocity distribution of SNAP_GPR56 proteins in unstimulated MIN6 β-cells. n = 133,312 SNAP_GPR56 receptors from 3 experiments. **D**. Classification of SNAP_GPR56 receptors based on the speed of their trajectories. Receptors with an average track speed of 0−1 μm/s were classified as stationary or immobile, 1−5 μm/s as slow, and >5 μm/s as fast. n = 2,201 tracks, from 3 experiments. **E**. A plot of mean track speed of SNAP_GPR56 against track duration, n = 2,201 tracks from 3 experiments. **F**. Confocal microscopy images showing expression of SNAP_GPR56 and endosomal markers Rab5a and transferrin receptor. Scale bar = 10 μm **G**. Scatter plot (upper) shows SNAP_GPR56 and Rab5a pixel intensities for 12 MIN6 β-cells co-expressing both plasmids. Bar graph (lower) shows colocalisation analysis of SNAP_GPR56 with Rab5a and transferrin receptors in MIN6 β-cells using Mander's colocalisation co-efficient, n = 3 experiments.

MIN6 β-cells responded to ATP, a purinergic receptor agonist that mobilises calcium from the endoplasmic reticulum, and tolbutamide, an ATP-sensitive potassium channel blocker [39,40], with elevations in intracellular calcium ([Ca^{2+}]i) levels (Suppl. Fig. 3a) and no statistically significant differences to peak responses in their basal (p > 0.2; Suppl. Fig. 3b). ATP and tolbutamide also elicited elevations in [Ca^{2+}]i in Gpr56KO-MIN6 β-cells transfected with SNAP_Gpr56 (Suppl. Fig. 3c), demonstrating that β-cell calcium signalling pathways were intact following SNAP_Gpr56 transfection. In native and Gpr56KO-MIN6 β-cells, 20 mmol/l glucose stimulated an increase in [Ca^{2+}]i (Suppl. Fig. 3d), indicating that their metabolic capacity was not compromised following Gpr56 deletion. P7 caused a rapid increase in [Ca^{2+}]i in native MIN6 β-cells, but it failed to increase [Ca^{2+}]i in Gpr56KO-MIN6 β-cells (Suppl. Fig. 3d), consistent with P7 acting in a GPR56-dependent manner in MIN6 β-cells. Similarly, P7 elicited increases in [Ca^{2+}]i in Gpr56KO-MIN6 β-cells transfected with SNAP_Gpr56 (Suppl. Fig. 3e) demonstrating that the transfected GPR56 is functional following SNAP-tag fusion.

A super-resolution iSIM microscopy imaging of Gpr56KO-MIN6 β-cells transfected with SNAP_Gpr56 and labelled with SNAP-Surface® 549 showed GPR56 localised to the plasma membrane and GPR56 constitutively trafficked to and from the cytoplasm (Figure 3B, and Suppl. Video 1), similar to fixed cells. Cells were visualised for 45 min following SNAP-Surface® 549 labelling and demonstrated that fluorescence was mainly at the plasma membrane at 10 min, whereas increased cytoplasmic fluorescence was evident at 20 and 45 min (Suppl. Fig. 3f). Suppl. Video 1 shows that some GPR56 molecules moved from the plasma membrane to the cytoplasm, whereas others were recycled from the cytoplasm back to the plasma membrane. Of those receptors that were not recycled to the plasma membrane, the majority moved slowly and remained within the cytoplasm. These observations are consistent with their velocity distribution (Figure 3C), in which the majority of the receptors were moving at a velocity of <5 μm/s, whereas others disappeared from the imaging focal plane. SNAP_GPR56 movement could be classified into three different states based on the average track speed of the labelled molecules (Figure 3D). Thus, some of the receptors were practically immobile, with average track speeds of 0—1 μm/s. Other receptors, accounting for 65.1% of the total trajectories, had average track speeds of 1—5 μm/s and were classified as slow, whereas the fast-moving receptors had average track speeds of >5 μm/s (Figure 3D). The fast-moving SNAP-GPR56 proteins were short-lived, with track durations of <1 s, whereas the receptors classified as immobile (0—1 μm/s) had the longest track durations (Figure 3E). However, there was no correlation between the speed of the movement of labelled SNAP_GPR56 molecules within a track and the track duration (r = - 0.19).

We co-transfected SNAP_Gpr56 with a fusion construct of the early endosomal markers Rab5a and GFP to investigate the intracellular compartment to which constitutively active GPR56 traffics. Confocal microscopy showed a strong colocalisation of constitutively trafficked SNAP_GPR56 with Rab5a (Figure 3F, upper panel and Figure 3G; Mander's colocalisation co-efficient of 0.86 ± 0.02), suggesting that approximately 86% of SNAP_GPR56 colocalised with Rab5a-positive endosomes. We also investigated the colocalisation of SNAP_GPR56 with transferrin receptors to determine whether constitutively internalised SNAP_GPR56 is recycled back to the plasma membrane, as transferrin receptors preferentially traffic via the recycling pathway [41]. Immunostaining for transferrin receptors (Figure 3F, lower panel) showed colocalisation with SNAP_GPR56 (Mander's colocalisation co-efficient of 0.66 ± 0.10, Figure 3G, lower panel), indicating that SNAP_GPR56 constitutively internalises through recycling endosomes.

Supplementary video related to this article can be found at doi: https://doi.org/10.1016/j.molmet.2021.101285

3.3. Constitutive GPR56 activity in β-cells reduces apoptosis

Constitutive GPCR activity, which has been described for several GPCRs [42,43], arises from an equilibrium between active and inactive receptor conformations, allowing receptor activation in the absence of an agonist. The overexpression of GPCRs allows agonist-independent downstream signalling of the active receptors to be more readily detectable [44,45]. To determine whether the constitutive activity of GPR56 affects β-cell function, we transfected a plasmid encoding full length, untagged Gpr56 into MIN6 β-cells to increase the number of active conformers, a method that has previously been used to investigate the activity of other aGPCRs, including GPR56, GPR133, GPR114, and EMR2 [18,46,47]. Quantitative PCR showed a significant upregulation (p < 0.0001) of Gpr56 mRNA levels at 24 and 48 h post-transfection, with the maximum expression obtained with a 1.2 μg plasmid at 48 h (Figure 4A). GPR56 protein upregulation was confirmed by western blotting (Figure 4B and C). The overexpression of Gpr56 did not affect basal insulin secretion (Figure 4D), consistent with our earlier observations of the collagen III activation of GPR56 not coupling to the stimulation of insulin secretion in the presence of a sub-stimulatory concentration of glucose [24]. However, basal apoptosis was significantly reduced in MIN6 β-cells following Gpr56 upregulation, but the overexpression of Gpr56 did not significantly reduce cytokine-induced apoptosis (Figure 4E). The deletion of Gpr56 in MIN6 β-cells led to a significant increase in caspase 3/7 activities induced by cytokines without significantly affecting basal apoptosis (Figure 4F).

3.4. Agonist stimulation further drives GPR56 internalisation in β-cells

Our identification of a high degree of the constitutive trafficking of GPR56 in β-cells led us to explore whether further internalisation could be driven by exposing β-cells to GPR56 agonists. Initial agonist-induced GPCR trafficking experiments were performed using SNAP_GLP1R-MIN6 β-cells, as GLP1R internalisation is well-characterised following exendin-4 stimulation [16,38,48]. As expected, the addition of 100 nmol/l exendin-4 to SNAP_GLP1R-MIN6 β-cells led to a robust internalisation of GLP1R after 30 min of agonist stimulation compared to cells exposed to the physiological buffer alone (Figure 5A). The extent of trafficking is evident from the line histograms that show fluorescence intensity along the yellow lines drawn across the control and treated cells: two distinct plasma membrane peaks were visible for the control, whereas multiple peaks were obtained after the exendin-4-stimulated receptor redistribution.

Similar trafficking experiments were also performed in which labelled SNAP_GPR56-MIN6 β-cells were incubated in a buffer for 30 min in the absence or presence of the GPR56 ligand collagen III. As we had observed previously, the widespread internalisation of GPR56 was observed in the absence of an agonist. However, GPR56 internalisation was further increased when the cells were exposed to 100 nmol/l collagen III (Figure 5B), and a 30-min incubation of MIN6 β-cells with collagen III led to an 86.0 ± 2.8% internalisation of GPR56 receptors compared to 50.9 ± 7.9% in the unstimulated state (Figure 5C). In contrast, the short peptide agonist of GPR56, P7, failed to promote GPR56 internalisation beyond those observed following incubation for 30 min in the physiological buffer alone (Figure 5D and E).

3.5 P7 increases intracellular calcium, promotes glucose-stimulated insulin secretion and reduces apoptosis in human islets

We have previously shown that the activation of β-cell GPR56 by collagen III is coupled to changes in [Ca^{2+}]i [24], a second messenger
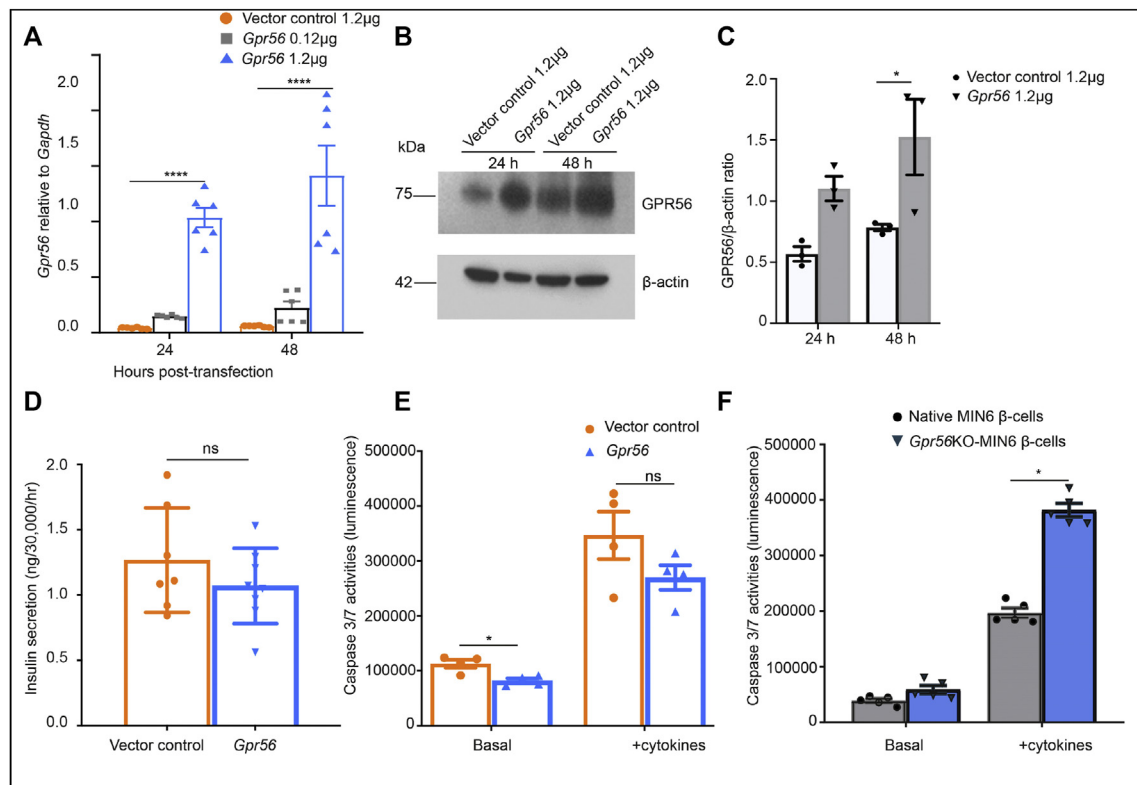
Figure 4: Effects of overexpression and deletion of *Gpr56* on MIN6 β-cell apoptosis. A. MIN6 β-cells were transiently transfected with empty vector or 0.12 μg and 1.2 μg of *Gpr56* plasmid DNA using lipofectamine and maintained in culture for 24 or 48 h cDNAs were prepared, and expression of *Gpr56* mRNA was quantified by qPCR relative to *Gapdh* in the same samples. Data are mean ± SEM, n = 6, ****p < 0.0001, two-way ANOVA with Tukey post-host test. **B**. Western blot image showing GPR56 protein in MIN6 β-cells transfected with empty vector or *Gpr56* plasmid for 24 and 48 h. Immunoblotting for β-actin in the same samples served as a loading control. **C**. Densitometric analysis of the relative protein level of GPR56 to β-actin in vector control and GPR56 overexpression in MIN6 β-cells at 24 and 48 h, n = 3 independent experiments, *p < 0.05, two-way ANOVA with Sidak's multiple comparisons test. At 48 h post-transfection, functional studies were carried out to determine the effect of overexpressing *Gpr56* on: **D**. basal insulin secretion, determined by radioimmunoassay, n = 8, ns = not significant, and **E**. basal and cytokine-induced apoptosis by measuring caspase 3/7 activities, n = 4. Data are mean ± SEM, *p < 0.05, two-way ANOVA with Tukey post-host test. **F**. Caspase 3/7 activities of native MIN6 β-cells and Gpr56KO-MIN6 β-cells were measured by a luminescence-based assay, n = 5. Data are mean ± SEM, *p < 0.05, two-way ANOVA with Tukey post-host test.

downstream of G_q and $G_{12/13}$ pathways, and the data presented here demonstrate that the peptide agonist P7 also increases $[Ca^{2+}i]$ in MIN6 β-cells in a GPR56-dependent manner (Suppl. Fig 3d). Therefore, we extended our functional analyses beyond MIN6 β-cells to assess the effect of P7 on $[Ca^{2+}]i$ in Fura-2 loaded human islet β-cells. Live-cell calcium imaging showed that 100 μmol/l P7 enhanced the elevation in the $[Ca^{2+}]i$ obtained in response to 20 mmol/l glucose, leading to a significantly higher basal to peak ratio (Figure 6A). As increased $[Ca^{2+}]i$ is a powerful stimulus for insulin exocytosis, we also investigated the effect of P7 on insulin secretion from human islets in a temperature-controlled perifusion system. As expected, 20 mmol/l glucose significantly stimulated insulin secretion, and the addition of 100 μmol/l P7 produced a rapid, sustained, and reversible increase in the plateau phase of glucose-induced insulin secretion above the results obtained in the presence of the 0.1% DMSO vehicle control (Figure 6B). The AUC analysis throughout P7 administration (34—54 min) in three separate experiments indicated a statistically significant stimulation by P7 above the response to 20 mmol/l glucose alone (Figure 6C). We also investigated the effect of P7 and collagen III on the apoptosis of human islets by quantifying caspase 3/7 activities. A pre-treatment of human islets with 100 μmol/l P7 or 100 nmol/l collagen III did not affect basal apoptosis, but collagen III significantly inhibited apoptosis induced by mixed cytokines. Though P7 caused a 30.6 ± 11.8% reduction in

cytokine-induced apoptosis in three separate experiments, this reduction was not statistically significant (p = 0.11; Figure 6D).

4. DISCUSSION

The canonical cycle of GPCR activation, internalisation, and recycling begins with the binding of an agonist to a cell-surface GPCR, conformational changes, and the dissociation of heterotrimeric G proteins, allowing the subunits to interact with downstream targets. Continuous agonist exposure is followed by phosphorylation by G-protein coupled receptor kinases, leading to receptor internalisation, in which the endocytosed GPCR can continue to signal [13], be ubiquitinylated for degradation, or be recycled back to the plasma membrane and be ready for another round of receptor activation [49]. Here, we used SNAP-tag labelling and super-resolution microscopy to demonstrate, for the first time, that the adhesion GPCR GPR56 is internalised and recycled independently of an agonist *in vitro*, with evidence of internalised receptors trafficking to the endosomal compartments. The velocities of the trafficked receptors were highly heterogeneous, with a majority of the GPR56 present on the plasma membrane or the early endosomes being stationary or slowly moving, whereas the fast-moving receptors were short-lived.
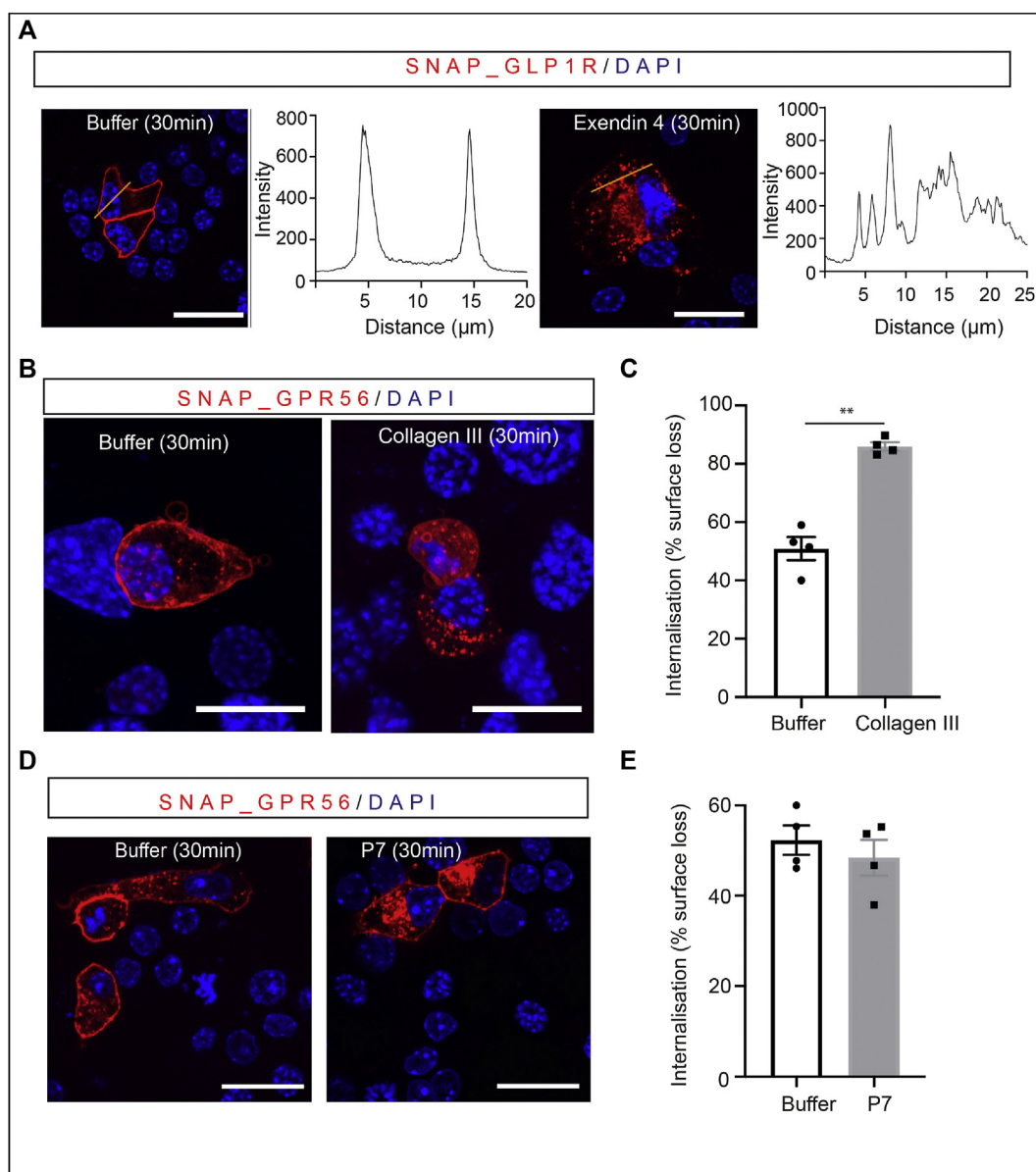
Figure 5: Agonist-dependent GPCR internalisation in MIN6 β-cells. A. Representative confocal images of MIN6 β-cells transfected with SNAP_*Glp1r* and labelled with SNAP-Surface® 549, after 30min incubation in the absence (left image) or presence (right image) of 100 nmol/l exendin-4. The line histograms show mean GLP1R intensity along the yellow lines drawn across the plasma membrane in buffer alone or after exendin-4 stimulation. Scale bar = 20 μm **B**. Representative confocal images of MIN6 β-cells transfected with SNAP_*Gpr56* and labelled with SNAP-Surface® 549, after 30 min incubation in the absence (left image) or presence (right image) of 100 nmol/l soluble collagen III. The control medium contains the collagen III vehicle (10 mmol/l HCl, buffered to pH 7.4). Scale bar = 20 μm **C**. Percentage internalisation of surface GPR56 in the absence and presence of 100 nmol/l collagen III. Data are mean ± SEM, n = 4 separate experiments, **p < 0.01, unpaired t-test. **D**. Representative confocal images of MIN6 β-cells transfected with SNAP_*Gpr56* and labelled with SNAP-Surface® 549, after 30 min incubation in the absence (left image) or presence (right image) of 1 mmol/l P7. The control medium contains the P7 vehicle (0.1% DMSO). Scale bar = 20 μm **E**. Percentage internalisation of surface GPR56 in the absence and presence of 1 mmol/l P7. Data are mean ± SEM, n = 4 separate experiments.

Constitutive internalisation is primarily a consequence of clathrin-independent endocytosis and, for many GPCRs, it has not been clear whether this internalisation is distinct from agonist-dependent endocytosis. This effect is further compounded by the possibility of having unidentified omnipresent ligands, such as ions and amino acids, in culture media, which are particularly relevant for the nutrient-sensing class C GPCRs [50,51]. We have recently shown that MIN6 β-cells do not synthesise collagen III [24]. Therefore, the constitutive signalling we observed for GPR56 was not due to the presence of locally produced collagen III.

However, β-cells are reported to synthesise other ligands such as transglutaminase 2 (TG2) and tetraspanin proteins, which can interact with GPR56. TG2 is a cross-linking enzyme that binds GPR56 in melanoma [52] and oligodendrocyte precursor cells [53], and it requires the presence of laminin to activate GPR56 [53,54]. Though direct binding with GPR56 has been demonstrated [55], it is unclear whether TG2 alone is a GPR56 agonist, as no downstream signalling has been described. The tetraspanin proteins CD9 and CD81 are reported to stabilise GPR56 in a G-protein complex with $G_{\alpha q/11}$ [20], though the function of this
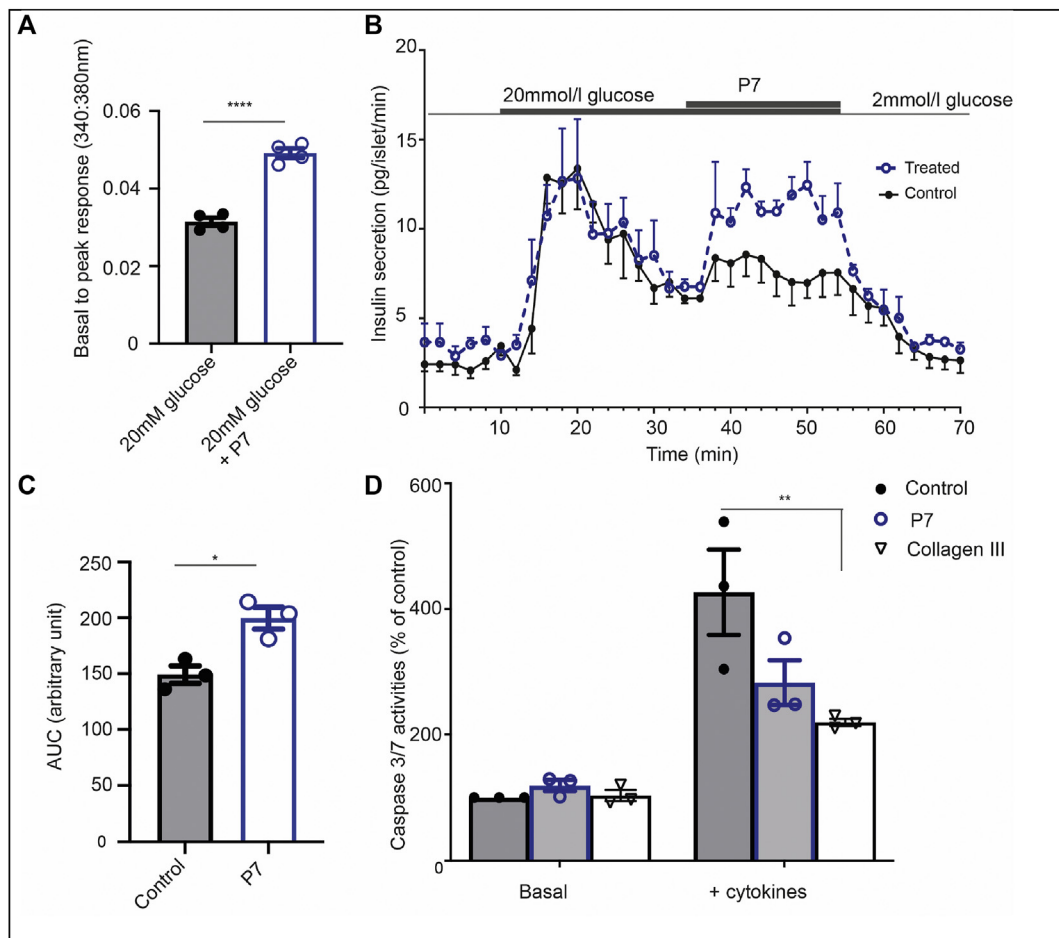
Figure 6: GPR56 agonist-mediated signalling in human islets. A. Dispersed human islet cells were loaded with Fura-2AM before being perifused with physiological solution containing 20 mmol/l glucose in the absence and presence of 100 μmol/l P7. Data are expressed as basal to peak changes in intracellular calcium, mean ± SEM, n = 4 experiments, ****p < 0.0001, unpaired t-test. **B**. Human islets were perifused with physiological solution containing 20 mmol/l glucose in the absence and presence of 100 μmol/l P7, as indicated (open circles), and control islets were perifused with vehicle (0.1% DMSO) instead of P7 (closed circles). Insulin secretion was quantified by radioimmunoassay. Data are mean + SEM, n = 4 replicates of 60 human islets, representative of 3 experiments with separate human islet donors. **C**. AUC insulin secretion data for 20 min exposure to 0.1% DMSO (Control) or 100 μmol/l P7, in the presence of 20 mmol/l glucose. Data are mean ± SEM, n = 3 experiments, *p < 0.05, unpaired t-test. **D**. Human islets were maintained in RPMI containing a cytokine cocktail or cytokine-free RPMI in the absence or presence of collagen III or P7. Apoptosis was determined by luminescence assay of caspase 3/7 activities. Data are mean ± SEM, n = 3 separate experiments, **p < 0.01, two-way ANOVA with Bonferroni's posthoc test.

interaction on GPR56 signalling is not yet known. Thus, given that there is no evidence that TG2 or tetraspanins are direct activators of GPR56 and that they are secreted from β-cells to reach the concentrations in the incubating medium capable of forming scaffolds, it might account for the rapid GPR56 internalisation we observed. Constitutive internalisation is the most likely explanation of our observations.

Constitutive GPR56 internalisation could be due to β-arrestin recruitment as another aGPCR, GPR64, mobilised β-arrestin 1 and 2 when its N-terminal fragment was removed [56], and this interaction with β-arrestins was enhanced by the addition of GPR64 peptide agonists [57]. It is known that constitutively active receptors are particularly attracted to β-arrestins [58,59], and these observations with GPR64 implicate the β-arrestin pathway in aGPCR internalisation. Indeed, it has been previously reported that full-length GPR56 and GPR56 with a truncated N-terminal fragment constitutively associated with β-arrestin 2, with the truncated GPR56 receptor exhibiting robust $G_{12/13}$ signalling in the absence of an agonist [11,18]. It is likely that GPR56-β-arrestin 2 complexes will allow sustained signalling in the endosomal compartments, as described for GPR64 [56] and some of the

Class B GPCRs [60]. Research efforts are focused on understanding the functional consequences of constitutive GPCR signalling [42,61,62], and it has recently been established that constitutively active GPR3 drives cold-induced thermogenesis intrinsically. In addition, GPR3 overexpression in adipocytes is sufficient to counteract metabolic dysfunction in mice [63].

Recent studies have shown that several aGPCRs exhibit some degree of constitutive signalling, independently of agonists [46,64,65]. However, progress in this area is limited, as 27 out of the 33 aGPCRs are orphans [66,67], and the extent to which the activity and function of the entire aGPCR class are influenced by constitutive internalisation remains elusive. As GPR56 in native β-cells *in vivo* is constantly exposed to collagen III in the extracellular matrix and vascular endothelial cells [24], GPR56 has likely adopted a constitutive recycling mechanism via the recycling endosomes to avoid overstimulation while maintaining a pool of receptors at the cell surface. We have shown here that constitutive GPR56 internalisation is potentially beneficial to β-cell health, as basal apoptosis, which reflects the low levels of unstimulated cell death in the absence of exogenous pro-apoptotic stimuli, was

decreased when *Gpr56* was overexpressed in MIN6 β-cells, and the deletion of *Gpr56* rendered MIN6 β-cells more susceptible to cytokine-induced apoptosis. This finding is consistent with observations made in a recent study, in which GPR56 overexpression in HEK-293T cells induced constitutive phosphorylation of paxillin [68], known to reduce apoptosis [69]. The recruitment of β-arrestins by constitutively active GPR56 could also play a role in this protection against apoptosis, as the co-transfection of β-arrestin 2 with constitutively active GPR56 has previously been shown to reduce cytotoxicity [18]. In a translational context, targeting GPR56 to reduce β-cell apoptosis has the capacity to maintain functional β-cell mass in diabetes.

Furthermore, an agonist-driven internalisation of GPR56 was observed when collagen III, the endogenous GPR56 ligand, was added. However, GPR56 internalisation above the background constitutive trafficking was not observed in the presence of P7, a synthetic GPR56 partial agonist. Despite not promoting GPR56 internalisation in MIN6 β-cells transfected with SNAP_*Gpr56*, P7 acted as a GPR56 agonist in MIN6 β-cells, as it elevated [Ca^{2+}]i, an effect that was lost following CRISPR-Cas9-mediated *Gpr56* deletion. Moreover, P7 also increased [Ca^{2+}]i in human islets and potentiated glucose-induced insulin secretion. Our observations demonstrate that though collagen III and P7 are both GPR56 agonists, they can have differing effects on GPR56 trafficking and signalling and suggest that GPR56 may have distinct regulatory mechanisms depending on the binding properties of the agonists. These differences may depend on whether GPR56 is in a full-length or truncated form. Thus, collagen III requires the presence of the GPR56 Stachel region to activate the receptor, whereas the synthetic P19 agonist, a longer version of P7, acts with or without the Stachel region [54].

The already high basal internalisation may explain why the partial agonist P7 was unable to internalise GPR56 further, as a negative correlation has been observed for receptors with high levels of constitutive signalling and the extent of agonist-induced internalisation [45]. A further understanding of the mechanisms involved will depend on identifying whether endogenous GPR56 exists in both full-length and truncated forms in MIN6 β-cells and the availability of GPR56-selective antagonists or inverse agonists. Similar to the μ-opioid GPCR, in which agonists have differential effects on activity and receptor internalisation, it is likely that P7 does not promote β-arrestin-2 recruitment, as it does not promote GPR56 internalisation. Thus, despite both being μ-opioid agonists, etorphine promotes receptor desensitisation and tolerance, whereas herkinorin does not cause receptor internalisation or recruit β-arrestin-2 [70]. Drugs that can activate a GPCR without inducing internalisation may be promising in separating therapeutic effects from unwanted side effects.

In summary, our data demonstrate that GPR56 is constitutively internalised, with potentially beneficial effects on β-cell health by reducing apoptosis. The synthetic GPR56 partial agonist, P7, does not induce GPR56 internalisation in β-cells and may be classed as a biased agonist, whereas the naturally occurring ligand, collagen III, robustly induced GPR56 internalisation. The constitutive trafficking property of GPR56 may be a mechanism of recycling non-activated receptors to the β-cell plasma membrane, in which they can bind to collagen III in the extracellular matrix when required. Furthermore, the agonist-mediated activation of β-cell GPR56, which can occur independently of receptor trafficking, is physiologically relevant in augmenting insulin secretion and protecting against apoptosis.

AUTHOR CONTRIBUTIONS

Research design: OEO, DJH, AK, PMJ, SJP. Conducted experiments: OEO, JC, JA, AA. Performed data analysis: OEO, SJP. Provided materials: PA, JA, DJH, JB. Wrote or contributed to the writing of the manuscript: OEO, SJP. All authors revised the manuscript critically for important intellectual content and approved the current version to be published. OEO and SJP are the guarantors of this work and, as such, had full access to all the data in the study and take responsibility for the integrity of the data and the accuracy of the data analysis.

DATA AVAILABILITY

SNAP_*Gpr56* is available for academic purposes. Further information and requests for reagents and resources should be directed to and will be fulfilled by the lead contact, Professor Shanta Persaud (shanta. persaud@kcl.ac.uk).

ACKNOWLEDGEMENTS

CONFLICTS OF INTEREST

The authors declare that they have no conflict of interest.

APPENDIX A. SUPPLEMENTARY DATA

Supplementary data to this article can be found online at https://doi.org/10.1016/j.molmet.2021.101285.

REFERENCES

[1] Araç, D., Boucard, A.A., Bolliger, M.F., Nguyen, J, Soltis, S.M., Südhof, T.C., et al., 2012. A novel evolutionarily conserved domain of cell-adhesion GPCRs mediates autoproteolysis. The EMBO Journal 31:1364—1378. https://doi.org/10.1038/emboj.2012.26.

[2] Hamann, J., Aust, G., Araç, D., Engel, F.B., Formstone, C., Fredriksson, R., et al., 2015. International union of basic and clinical pharmacology. XCIV. Adhesion G protein-coupled receptors. Pharmacological Reviews 67:338—367. https://doi.org/10.1124/pr.114.009647.

[3] Luo, R., Jeong, S.-J., Yang, A., Wen, M., Saslowsky, D.E., Lencer, W.I, et al., 2014. Mechanism for adhesion G protein-coupled receptor GPR56-mediated RhoA activation induced by collagen III stimulation. PloS One 9:e100043. https://doi.org/10.1371/journal.pone.0100043.

[4] Monk, K.R., Hamann, J., Langenhan, T., Nijmeijer, S., Schöneberg, T., Liebscher, I., 2015. Adhesion G protein-coupled receptors: from in vitro pharmacology to in vivo mechanisms. Molecular Pharmacology 88:617—623. https://doi.org/10.1124/mol.115.098749.

[5] Liebscher, I., Schön, J., Petersen, S.C., Fischer, L., Auerbach, N., Demberg, L.M., et al., 2014. A tethered agonist within the ectodomain activates the adhesion G protein-coupled receptors GPR126 and GPR133. Cell Reports 9:2018—2026. https://doi.org/10.1016/j.celrep.2014.11.036.

[6] Demberg, L.M., Winkler, J., Wilde, C., Simon, K-U., Schön, J., Rothemund, S., et al., 2017. Activation of adhesion G protein-coupled receptors: agonist specificity OF stachel sequence-derived peptides. Journal of Biological Chemistry 292:4383—4394. https://doi.org/10.1074/jbc.M116.763656.

[7] Demberg, L.M., Rothemund, S., Schöneberg, T., Liebscher, I., 2015. Identification of the tethered peptide agonist of the adhesion G protein-coupled

receptor GPR64/ADGRG2. Biochemical and Biophysical Research Communications 464:743—747. https://doi.org/10.1016/j.bbrc.2015.07.020.

[8] Stoveken, H.M., Bahr, L.L., Anders, M.W., Wojtovich, A.P., Smrcka, A.V., Tall, G.G., 2016. Dihydromunduletone is a small-molecule selective adhesion G protein-coupled receptor antagonist. Molecular Pharmacology 90:214—224. https://doi.org/10.1124/mol.116.104828.

[9] Schöneberg, T., Liebscher, I., Luo, R., Monk, K.R., Piao, X., 2015. Tethered agonists: a new mechanism underlying adhesion G protein-coupled receptor activation. Journal of Receptors and Signal Transduction Research 35:220—223. https://doi.org/10.3109/10799893.2015.1072978.

[10] Stoveken, H.M., Hajduczok, A.G., Xu, L., Tall, G.G., 2015. Adhesion G protein-coupled receptors are activated by exposure of a cryptic tethered agonist. Proceedings of the National Academy of Sciences of the United States of America 112:6194—6199. https://doi.org/10.1073/pnas.1421785112.

[11] Kishore, A., Purcell, R.H., Nassiri-Toosi, Z., Hall, R.A., 2016. Stalk-dependent and stalk-independent signaling by the adhesion G protein-coupled receptors GPR56 (ADGRG1) and Bai1 (ADGRB1). Journal of Biological Chemistry 291: 3385—3394. https://doi.org/10.1074/jbc.M115.689349.

[12] Scholz, N., Guan, C., Nieberler, M., Grotemeyer, A., Maiellaro, I., Gao, S., et al., 2017. Mechano-dependent signaling by Latrophilin/CIRL quenches cAMP in proprioceptive neurons. Elife 6:e28360. https://doi.org/10.7554/eLife.28360.

[13] Calebiro, D., Nikolaev, V.O., Gagliani, M.C., de Filippis, T., Dees, C., Tacchetti, C., et al., 2009. Persistent cAMP-signals triggered by internalized G-protein-coupled receptors. PLoS Biology 7:e1000172. https://doi.org/10.1371/journal.pbio.1000172.

[14] Leyris, J.-P., Roux, T., Trinquet, E., Verdié, P., Fehrentz, J-A., Oueslati, N., et al., 2011. Homogeneous time-resolved fluorescence-based assay to screen for ligands targeting the growth hormone secretagogue receptor type 1a. Analytical Biochemistry 408:253—262. https://doi.org/10.1016/j.ab.2010.09.030.

[15] Podewin, T., Ast, J., Broichhagen, J., Fine, N.H.F., Nasteska, D., Leippe, P., et al., 2018. Conditional and reversible activation of class A and B G protein-coupled receptors using tethered pharmacology. ACS Central Science 4:166—179. https://doi.org/10.1021/acscentsci.7b00237.

[16] Ast, J., Arvaniti, A., Fine, N.H.F., Nasteska, D., Ashford, F.B., Stamataki, Z., et al., 2020. Super-resolution microscopy compatible fluorescent probes reveal endogenous glucagon-like peptide-1 receptor distribution and dynamics. Nature Communications 11:467. https://doi.org/10.1038/s41467-020-14309-w.

[17] Poc, P., Gutzeit, V.A., Ast, J., Lee, J., Jones, B.J., D'Este, E., et al., 2020. Interrogating surface versus intracellular transmembrane receptor populations using cell-impermeable SNAP-tag substrates. Chemical Science 11:7871—7883. https://doi.org/10.1039/D0SC02794D.

[18] Paavola, K.J., Stephenson, J.R., Ritter, S.L., Alter, S.P., Hall, R.A., 2011. The N terminus of the adhesion G protein-coupled receptor GPR56 controls receptor signaling activity. Journal of Biological Chemistry 286:28914—28921. https://doi.org/10.1074/jbc.M111.247973.

[19] Karpus, O.N., Veninga, H., Hoek, R.M., Flierman, D., van Buul, J.D., Vandenakker, C.C, et al., 2013. Shear stress-dependent downregulation of the adhesion-G protein-coupled receptor CD97 on circulating leukocytes upon contact with its ligand CD55. The Journal of Immunology 190:3740—3748. https://doi.org/10.4049/jimmunol.1202192.

[20] Little, K.D., Hemler, M.E., Stipp, C.S., 2004. Dynamic regulation of a GPCR-tetraspanin-G protein complex on intact cells: central role of CD81 in facilitating GPR56-Galpha q/11 association. Molecular Biology of the Cell 15:2375—2387. https://doi.org/10.1091/mbc.E03-12-0886.

[21] Amisten, S., Atanes, P., Hawkes, R., Ruz-Maldonado, I., Liu, B., Parandeh, F., et al., 2017. A comparative analysis of human and mouse islet G-protein

coupled receptor expression. Scientific Reports 7:46600. https://doi.org/10.1038/srep46600.

[22] Amisten, S., Salehi, A., Rorsman, P., Jones, P.M., Persaud, S.J., 2013. An atlas and functional analysis of G-protein coupled receptors in human islets of Langerhans. Pharmacology & Therapeutics 139:359—391. https://doi.org/10.1016/j.pharmthera.2013.05.004.

[23] Luo, R., Jeong, S.-J., Jin, Z., Strokes, N., Li, S., Piao, X., 2011. G protein-coupled receptor 56 and collagen III, a receptor-ligand pair, regulates cortical development and lamination. Proceedings of the National Academy of Sciences of the United States of America 108:12925—12930. https://doi.org/10.1073/pnas.1104821108.

[24] Olaniru, O.E., Pingitore, A., Giera, S., Piao, X., Castañera González, R., Jones, P.M., et al., 2018. The adhesion receptor GPR56 is activated by extracellular matrix collagen III to improve β-cell function. Cellular and Molecular Life Sciences 75:4007—4019. https://doi.org/10.1007/s00018-018-2846-4.

[25] Dunér, P., Al-Amily, I.M., Soni, A., Asplund, O., Safi, F., Storm, P., et al., 2016. Adhesion G protein-coupled receptor G1 (ADGRG1/GPR56) and pancreatic β-cell function. The Journal of Cinical Endocrinology and Metabolism 101:4637—4645. https://doi.org/10.1210/jc.2016-1884.

[26] Sun, X., Zhang, A., Baker, B., Sun, L., Howard, A., Buswell, J., et al., 2011. Development of SNAP-tag fluorogenic probes for wash-free fluorescence imaging. ChemBioChem 12:2217—2226. https://doi.org/10.1002/cbic.201100173.

[27] Gibson, D.G., Young, L., Chuang, R.-Y., Venter, J.C., Hutchison, C.A, Smith, H.O., et al., 2009. Enzymatic assembly of DNA molecules up to several hundred kilobases. Nature Methods 6:343—345. https://doi.org/10.1038/nmeth.1318.

[28] Atanes, P., Ruz-Maldonado, I., Hawkes, R., Liu, B., Persaud, S.J, Amisten, S., 2018. Identifying signalling pathways regulated by GPRC5B in β-cells by CRISPR-cas9-mediated genome editing. Cellular Physiology and Biochemistry 45:656—666. https://doi.org/10.1159/000487159.

[29] Smith, P.K., Krohn, R.I., Hermanson, G.T., Mallia, A.K., Gartner, F.H, Provenzano, M.D., et al., 1985. Measurement of protein using bicinchoninic acid. Analytical Biochemistry 150:76—85. https://doi.org/10.1016/0003-2697(85)90442-7.

[30] McCloy, R.A., Rogers, S., Caldon, C.E., Lorca, T., Castro, A., Burgess, A., 2014. Partial inhibition of Cdk1 in G 2 phase overrides the SAC and decouples mitotic events. Cell Cycle 13:1400—1412. https://doi.org/10.4161/cc.28401.

[31] Stauffer, W., Sheng, H., Lim, H.N., 2018. EzColocalization: an ImageJ plugin for visualizing and measuring colocalization in cells and organisms. Scientific Reports 8:15764. https://doi.org/10.1038/s41598-018-33592-8.

[32] Dunn, K.W., Kamocka, M.M., McDonald, J.H., 2011. A practical guide to evaluating colocalization in biological microscopy. American Journal of Physiology - Cell Physiology 300:C723—C742. https://doi.org/10.1152/ajpcell.00462.2010.

[33] Tinevez, J.-Y., Perry, N., Schindelin, J., Hoopes, G.M., Reynolds, G.D., Laplantine, E., et al., 2017. TrackMate: an open and extensible platform for single-particle tracking. Methods 115:80—90. https://doi.org/10.1016/j.ymeth.2016.09.016.

[34] Pfaffl, M.W., 2001. A new mathematical model for relative quantification in real-time RT-PCR. Nucleic Acids Research 29:e45. https://doi.org/10.1093/nar/29.9.e45.

[35] Atanes, P., Ruz-Maldonado, I., Olaniru, O.E., Persaud, S.J., 2020. Assessing mouse islet function. Methods in Molecular Biology 2128:241—268. https://doi.org/10.1007/978-1-0716-0385-7_17.

[36] Pingitore, A., Gonzalez-Abuin, N., Ruz-Maldonado, I., Huang, G.C., Frost, G., Persaud, S.J., 2019. Short chain fatty acids stimulate insulin secretion and reduce apoptosis in mouse and human islets in vitro: role of free fatty acid

receptor 2. Diabetes, Obesity and Metabolism 21:330—339. https://doi.org/10.1111/dom.13529.

[37] Gey, G.O., Gey, M.K., 1936. The maintenance of human normal cells and tumor cells in continuous culture: I. preliminary report: cultivation of mesoblastic tumors and normal tissue and notes on methods of cultivation. American Journal of Cancer 27:45—76. https://doi.org/10.1158/ajc.1936.45.

[38] Roed, S.N., Wismann, P., Underwood, C.R., Kulahin, N., Iversen, H., Cappelen, K.A., et al., 2014. Real-time trafficking and signaling of the glucagon-like peptide-1 receptor. Molecular and Cellular Endocrinology 382:938—949. https://doi.org/10.1016/j.mce.2013.11.010.

[39] Jonkers, F.C., Guiot, Y., Rahier, J., Henquin, J.C., 2001. Tolbutamide stimulation of pancreatic beta-cells involves both cell recruitment and increase in the individual Ca(2+) response. British Journal of Pharmacology 133:575—585. https://doi.org/10.1038/sj.bjp.0704108.

[40] Khan, S., Yan-Do, R., Duong, E., Wu, X., Bautista, A., Cheley, S., et al., 2014. Autocrine activation of P2Y1 receptors couples Ca (2+) influx to Ca (2+) release in human pancreatic beta cells. Diabetologia 57:2535—2545. https://doi.org/10.1007/s00125-014-3368-8.

[41] Mayle, K.M., Le, A.M., Kamei, D.T., 2012. The intracellular trafficking pathway of transferrin. Biochimica et Biophysica Acta 1820:264—281. https://doi.org/10.1016/j.bbagen.2011.09.009.

[42] Berg, K.A., Harvey, J.A., Spampinato, U., Clarke, W.P., 2005. Physiological relevance of constitutive activity of 5-HT2A and 5-HT2C receptors. Trends in Pharmacological Sciences 26:625—630. https://doi.org/10.1016/j.tips.2005.10.008.

[43] Lau, P.N., Chow, K.B.S., Chan, C.-B., Cheng, C.H.K., Wise, H., 2009. The constitutive activity of the ghrelin receptor attenuates apoptosis via a protein kinase C-dependent pathway. Molecular and Cellular Endocrinology 299:232—239. https://doi.org/10.1016/j.mce.2008.12.006.

[44] Martin, A.L., Steurer, M.A., Aronstam, R.S., 2015. Constitutive activity among orphan class-A G protein coupled receptors. PloS One 10(1—12):e0138463. https://doi.org/10.1371/journal.pone.0138463.

[45] Hendrik Schmidt, J., Perslev, M., Bukowski, L., Stoklund, M., Herborg, F., Herlo, R., et al., 2019. Constitutive internalization across therapeutically targeted GPCRs correlates with constitutive activity. Basic and Clinical Pharmacology and Toxicology. https://doi.org/10.1111/bcpt.13274.

[46] Gupte, J., Swaminath, G., Danao, J., Tian, H., Li, Y., Wu, X., 2012. Signaling property study of adhesion G-protein-coupled receptors. FEBS Letters 586:1214—1219. https://doi.org/10.1016/j.febslet.2012.03.014.

[47] Bhudia, N., Desai, S., King, N., Ancellin, N., Grillot, D., Barnes, A.A., et al., 2020. G protein-coupling of adhesion GPCRs ADGRE2/EMR2 and ADGRE5/CD97, and activation of G protein signalling by an anti-EMR2 antibody. Scientific Reports 10:1004. https://doi.org/10.1038/s41598-020-57989-6.

[48] Jones, B., Buenaventura, T., Kanda, N., Chabosseau, P., Owen, B.M., Scott, R., et al., 2018. Targeting GLP-1 receptor trafficking to improve agonist efficacy. Nature Communications 9:1602. https://doi.org/10.1038/s41467-018-03941-2.

[49] Pavlos, N.J., Friedman, P.A., 2017. GPCR signaling and trafficking: the long and short of it. Trends in Endocrinology and Metabolism 28:213—226. https://doi.org/10.1016/j.tem.2016.10.007.

[50] Jacobsen, S.E., Ammendrup-Johnsen, I., Jansen, A.M., Gether, U., Madsen, K.L., Bräuner-Osborne, H., 2017. The GPRC6A receptor displays constitutive internalization and sorting to the slow recycling pathway. Journal of Biological Chemistry 292:6910—6926. https://doi.org/10.1074/jbc.M116.762385.

[51] Lee, M.J., Van Brocklyn, J.R., Thangada, S., Liu, C.H., Hand, A.R., Menzeleev, R., et al., 1998. Sphingosine-1-phosphate as a ligand for the G protein-coupled receptor EDG-1. Science 279:1552—1555. https://doi.org/10.1126/science.279.5356.1552.

[52] Xu, L., Begum, S., Hearn, J.D., Hynes, R.O., 2006. GPR56, an atypical G protein-coupled receptor, binds tissue transglutaminase, TG2, and inhibits melanoma tumor growth and metastasis. Proceedings of the National

Academy of Sciences of the United States of America 103:9023—9028. https://doi.org/10.1073/pnas.0602681103.

[53] Giera, S., Luo, R., Ying, Y., Ackerman, S.D., Jeong, S.J., Stoveken, H.M, et al., 2018. Microglial transglutaminase-2 drives myelination and myelin repair via GPR56/ADGRG1 in oligodendrocyte precursor cells. Elife 7:e33385. https://doi.org/10.7554/eLife.33385.

[54] Zhu, B., Luo, R., Jin, P., Li, T., Oak, H.C., Giera, S., et al., 2019. GAIN domain-mediated cleavage is required for activation of G protein-coupled receptor 56 (GPR56) by its natural ligands and a small-molecule agonist. Journal of Biological Chemistry 294:19246—19254. https://doi.org/10.1074/jbc.RA119.008234.

[55] Salzman, G.S., Zhang, S., Fernandez, C.G., Araç, D., Koide, S., 2020. Specific and direct modulation of the interaction between adhesion GPCR GPR56/ADGRG1 and tissue transglutaminase 2 using synthetic ligands. Scientific Reports 10:16912. https://doi.org/10.1038/s41598-020-74044-6.

[56] Azimzadeh, P., Talamantez-Lyburn, S.C., Chang, K.T., Inoue, A., Balenga, N., 2019. Spatial regulation of GPR64/ADGRG2 signaling by β-arrestins and GPCR kinases. Annals of the New York Academy of Sciences 1456:26—43. https://doi.org/10.1111/nyas.14227.

[57] Sun, Y., Zhang, D., Ma, M.-L., Lin, H., Song, Y., Wang, J., et al., 2020. Optimization of a peptide ligand for the adhesion GPCR ADGRG2 provides a potent tool to explore receptor biology. Journal of Biological Chemistry. https://doi.org/10.1074/jbc.RA120.014726.

[58] Ferrari, S.L., Bisello, A., 2001. Cellular distribution of constitutively active mutant parathyroid hormone (PTH)/PTH-related protein receptors and regulation of cyclic adenosine 3',5'-monophosphate signaling by beta-arrestin2. Molecular Endocrinology 15:149—163. https://doi.org/10.1210/mend.15.1.0587.

[59] Barak, L.S., Oakley, R.H., Laporte, S.A., Caron, M.G., 2001. Constitutive arrestin-mediated desensitization of a human vasopressin receptor mutant associated with nephrogenic diabetes insipidus. Proceedings of the National Academy of Sciences of the United States of America 98:93—98. https://doi.org/10.1073/pnas.011303698.

[60] Thomsen, A.R.B., Plouffe, B., Cahill, T.J., Shukla, A.K., Tarrasch, J.T., Dosey, A.M., et al., 2016. GPCR-G protein-β-arrestin super-complex mediates sustained G protein signaling. Cell 166:907—919. https://doi.org/10.1016/j.cell.2016.07.004.

[61] Mear, Y., Enjalbert, A., Thirion, S., 2013. GHS-R1a constitutive activity and its physiological relevance. Frontiers in Neuroscience 7:87. https://doi.org/10.3389/fnins.2013.00087.

[62] Meye, F.J., Ramakers, G.M.J., Adan, R.A.H., 2014. The vital role of constitutive GPCR activity in the mesolimbic dopamine system. Translational Psychiatry 4:e361. https://doi.org/10.1038/tp.2013.130.

[63] Sveidahl Johansen, O., Ma, T., Hansen, J.B., Markussen, L.K., Schreiber, R., Reverte-Salisa, L., et al., 2021. Lipolysis drives expression of the constitutively active receptor GPR3 to induce adipose thermogenesis. Cell. https://doi.org/10.1016/j.cell.2021.04.037.

[64] Wilde, C., Fischer, L., Lede, V., Kirchberger, J., Rothemund, S., Schöneberg, T., et al., 2016. The constitutive activity of the adhesion GPCR GPR114/ADGRG5 is mediated by its tethered agonist. The FASEB Journal 30:666—673. https://doi.org/10.1096/fj.15-276220.

[65] Paavola, K.J., Hall, R.A., 2012. Adhesion G protein-coupled receptors: signaling, pharmacology, and mechanisms of activation. Molecular Pharmacology 82:777—783. https://doi.org/10.1124/mol.112.080309.

[66] Alexander, S.P., Christopoulos, A., Davenport, A.P., Kelly, E., Marrion, N.V., Peters, J.A., et al., 2017. The concise guide to pharmacology 2017/18: G protein-coupled receptors. British Journal of Pharmacology 174(Suppl 1):S17—S129. https://doi.org/10.1111/bph.13878.

[67] Davenport, A.P., Alexander, S.P.H., Sharman, J.L., Pawson, A.J., Benson, H.E., Monaghan, A.E., et al., 2013. International Union of Basic and Clinical Pharmacology. LXXXVIII. G protein-coupled receptor list: recommendations for new pairings with cognate ligands. Pharmacological Reviews 65:967—986. https://doi.org/10.1124/pr.112.007179.

[68] Chatterjee, T., Zhang, S., Posey, T.A., Jacob, J., Wu, L., Yu, W., et al., 2021. Anti-GPR56 monoclonal antibody potentiates GPR56-mediated Src-Fak signaling to modulate cell adhesion. Journal of Biological Chemistry 296: 100261. https://doi.org/10.1016/j.jbc.2021.100261.

[69] Du, C., Wang, X., Zhang, J., Liu, X., Zhu, J., Liu, Y., 2016. Paxillin is positively correlated with the clinicopathological factors of colorectal cancer, and knockdown of Paxillin improves sensitivity to cetuximab in colorectal cancer cells. Oncology Reports 35:409—417. https://doi.org/10.3892/or.2015.4352.

[70] Groer, C.E., Tidgewell, K., Moyer, R.A., Harding, W.W., Rothman, R.B., Prisinzano, T.E., et al., 2007. An opioid agonist that does not induce mu-opioid receptor—arrestin interactions or receptor internalization. Molecular Pharmacology 71:549—557. https://doi.org/10.1124/mol.106.028258.